Chemical Engineering Science 133 (2015) 82–90

Contents lists available at ScienceDirect

Chemical Engineering Science

journal homepage: www.elsevier.com/locate/ces

Image-based monitoring for early detection of fouling in crystallisation processes

Christos Tachtatzis [a], Rachel Sheridan [b], Craig Michie [a], Robert C. Atkinson [a], Alison Cleary [a], Jerzy Dziewierz [c], Ivan Andonovic [a], Naomi E.B. Briggs [d], Alastair J. Florence [d], Jan Sefcik [b,*]

[a] Centre for Intelligent Dynamic Communications, Department of Electronic and Electrical Engineering, University of Strathclyde, Glasgow, Scotland G1 1XW, UK
[b] EPSRC Centre for Innovative Manufacturing in Continuous Manufacturing and Crystallisation, Department of Chemical and Process Engineering, University of Strathclyde, Glasgow, Scotland G1 1XJ, UK
[c] Centre for Ultrasonic Engineering, Department of Electronic and Electrical Engineering, University of Strathclyde, Glasgow, Scotland G1 1XW, UK
[d] EPSRC Centre for Innovative Manufacturing in Continuous Manufacturing and Crystallisation, Strathclyde Institute of Pharmacy and Biomedical Sciences, University of Strathclyde, Glasgow, Scotland G4 0RE, UK

HIGHLIGHTS

- Automatic algorithm to detect early stages of fouling.
- Distinguishing crystal appearance in the bulk solution and at the crystalliser walls.
- Online, real-time detection of induction time.

ARTICLE INFO

Article history:
Received 4 September 2014
Received in revised form
1 December 2014
Accepted 16 January 2015
Available online 28 January 2015

Keywords:
Continuous crystallisation
Fouling
Encrustation
Nucleation
Induction time
Imaging

ABSTRACT

Fouling or encrustation is a significant problem in continuous crystallisation processes where crystal deposits at surfaces impede heat transfer, increase flow resistance and reduce product quality. This paper proposes an automatic algorithm to detect early stages of fouling using images of vessel surfaces from commodity cameras. Statistical analysis of the pixel intensity variation offers the ability to distinguish appearance of crystals in the bulk solution and on the crystalliser walls. This information is used to develop a fouling metric indicator and determine separately induction times for appearance of first crystals at the surfaces and in the bulk. A method to detect process state changes using Bayesian online change point detection is also proposed, where the first change point is used to determine induction time either at the surface or in the bulk, based on real-time online measurements without using any predetermined threshold which usually varies between experiments and depends on data acquisition equipment. This approach can be used for in situ monitoring of early signs of encrustation to allow early warning for corrective actions to be taken when operating continuous crystallisation processes.

1. Introduction

Crystallisation is an important unit operation in chemical, pharmaceutical and food industries for isolation and purification of intermediates and final products. Fouling or encrustation in the context of crystallisation is the formation of crystal deposits on equipment surfaces, pipe walls and process analytical probes and occurs as a result of heterogeneous nucleation and/or attachment of crystals and their subsequent growth at solid surfaces (Bott, 1997; Mullin, 2001). Fouled surfaces impede heat transfer (Geddert et al., 2011a), increase flow resistance and decrease product quality (Wallhäußer et al., 2012). The impact of fouling and encrustation is even greater on continuous crystallisation processes where system blockages result in shutdowns leading to losses of time and revenue. Process conditions that influence fouling in crystallisation processes include solvent composition,

* Corresponding author.
E-mail addresses: christos.tachtatzis@strath.ac.uk (C. Tachtatzis), rachel.sheridan@strath.ac.uk (R. Sheridan), c.michie@strath.ac.uk (C. Michie), robert.atkinson@strath.ac.uk (R.C. Atkinson), alison.cleary@strath.ac.uk (A. Cleary), jerzy.dziewierz@strath.ac.uk (J. Dziewierz), i.andonovic@strath.ac.uk (I. Andonovic), naomi.briggs@strath.ac.uk (N.E.B. Briggs), alastair.florence@strath.ac.uk (A.J. Florence), jan.sefcik@strath.ac.uk (J. Sefcik).

http://dx.doi.org/10.1016/j.ces.2015.01.038
0009-2509/

supersaturation, pH, temperature, flow velocity and regime, additives or impurities, while interface conditions that affect fouling include surface energy, roughness and topography, number of nucleation sites and aging of the fouling layer (Geddert et al., 2009). Mechanisms of initiating encrustation have been studied previously, where a crystalline phase was nucleated on solid surfaces at controlled local supersaturation and without influence from particle attachment (Vendel and Rasmuson, 1997).

Common methods to mitigate fouling include mechanically altering the surface using methods such as ultrasound or scraping or chemically altering the surface using coatings to reduce the number of nucleation sites and/or remove attached crystals (Geddert et al., 2011b). Increasing the induction time for surface fouling can be achieved by changing the energy and topography of the surface or by changing the flow conditions (Förster et al., 1999). The rough surface can stabilise crystal nuclei and promote growth on the surface, while fouling is typically delayed at smoother surfaces.

A review of detection methods of fouling in the food industry can be found in the previous literature (Wallhäußer et al., 2012). Common, non-invasive methods to detect fouling are to monitor the hydrodynamic and heat transfer parameters. Hydrodynamic methods monitor the inlet and outlet pressures and infer the degree of deposits on the walls of a tube. Heat transfer methods monitor heat transfer losses to infer the degree of fouling. Both of these methods have low sensitivity and are generally not suitable for early stage monitoring of fouling in continuous crystallisers since significant fouling must occur before temperature or pressure variations are detectable. Other methods include the measurement of the electrical resistance or conductivity, ultrasound and vibration, however all these alter the fouling (i.e. fouled deposits may be broken off and then drift downstream). In the crystallisation domain it is common to use reflectance, turbidity and other spectroscopic methods to monitor processes in situ but none of these are specifically suited to provide direct information about the state of vessel walls and the presence or absence of fouling therein. For example, when turbidity probes are used to estimate nucleation induction time (Raphael and Rohani, 1996; Moscosa-Santillán et al., 2000), the method is unable to distinguish appearance of crystals in the liquid phase from that on vessel walls if and when fouling occurs.

Imaging is another technique commonly used to track various properties of multiphase systems containing suspended solid particles and/or bubbles (Oliveira et al., 2003), identify nucleation induction time (Simon et al., 2009a,b) or crystal growth (Brown and Ni, 2011) in industrial settings. A review of recent advances in monitoring and control of crystallisation systems using imaging can be found in Nagy et al. (2013). Use of in situ endoscopy-stroboscopy (Simon et al., 2012) equipment and multivariate image analysis for process monitoring has been demonstrated. Estimating nucleation induction time in the bulk through Bulk Video Imaging (Simon et al., 2010a) using multivariate image analysis and by converting pixel intensities time series of acoustic signals allows to eliminate stirrer effects through band-stop filtering in batch crystallisers. Methods to automatically estimate induction time using Shewhart Charts were shown in Simon et al. (2010a,b). These techniques apply to bulk monitoring only and to our knowledge there is no previously published method for detection of fouling through image analysis.

Fouling is an important problem in both batch and continuous crystallisation. It is especially significant for continuous crystallisation processes where early detection of fouling can be used to guide relevant corrective actions in order to keep process running. In this work a batch system has been designed which locally mimics the behaviour of a continuous plug-flow type crystallisation platform, in terms of keeping the local temperature and solution concentration constant, at least until the appearance of first crystals at walls or in the bulk. The approach proposed here is applicable subject to visual access to the crystalliser walls and uses an off-the-shelf commodity camera, pointing towards an area of interest at solid-liquid interface while looking through a transparent crystalliser wall.[1] Statistical analysis of the acquired images allows distinguishing crystal appearance in the bulk solution from fouling on the solid surfaces. Note that the induction times determined here refer to the location where crystals are observed and the appearance of crystals at that location does not necessarily mean that nucleation occurred there. The aim of the proposed technique is to separately determine induction times for appearance of crystals at solid surfaces and in the bulk automatically and in real-time, by providing a sensitive early warning system for detection of fouling in crystallisation processes.

2. Methodology

2.1. Experimental setup

The experimental setup used to monitor fouling at glass crystalliser walls under isothermal conditions was a batch system known as a moving fluid oscillatory baffled crystalliser (MFOBC). However, we note that the image-based monitoring and image analysis approach proposed here can be used to analyse data collected from any other experimental setup where real-time images of vessel walls are available, under batch or continuous, isothermal or non-isothermal conditions.

The MFOBC has orifice baffles spaced equally throughout the glass pipe which are overlaid with the direction of fluid oscillation (Ni et al., 2006). Local mixing is facilitated through eddy formation due to the interaction of the baffles with the oscillatory flow. The oscillation conditions are defined through frequency and amplitude (Stonestreet and Harvey, 2002). This system can achieve close to plug flow when operating under continuous conditions, as a continuous oscillatory baffled crystalliser (COBC), at relatively low net flow rates while good heat and mass transfer is radial direction as well as solid suspension is facilitated by oscillatory motions. In a typical COBC setup there are several glass sections operated under different temperatures and fouling is likely to occur in a section with highest supersaturation. In order to monitor the behaviour in such a section independent from the rest of the COBC setup, a physical batch model locally representing the COBC conditions was constructed by removing the section of interest from the continuous arrangement and mounting it vertically between two other sections providing suitable boundary conditions to prevent nucleation outside of the section of interest by keeping the temperature of the fluid outside of the section above saturation temperature. The resulting batch setup can reproduce local temperature, concentration and flow conditions identical to the relevant section of the COBC under corresponding conditions, in the absence of any solid phase until onset of crystal formation is observed.

The MFOBC used here (shown in Fig. 1) consists of tubular jacketed glass sections with orifice baffles spaced equally throughout. Each full glass section is made up of 22 individual cells of volume 5 ml and internal diameter 15 mm (DN15). The batch setup contains one half glass straight attached to bellows and kept at temperature $T1$, followed by one full straight where desired target temperature is kept at the position of monitoring cameras to achieve required supersaturation, and then another half straight at the top kept at temperature $T5$, completing the setup. The principle behind this configuration is that while all three regions are interconnected, the temperatures are calibrated so that the cameras are always monitoring regions of fixed temperature. The

[1] Industrial settings with opaque walls will require appropriate adjustments.

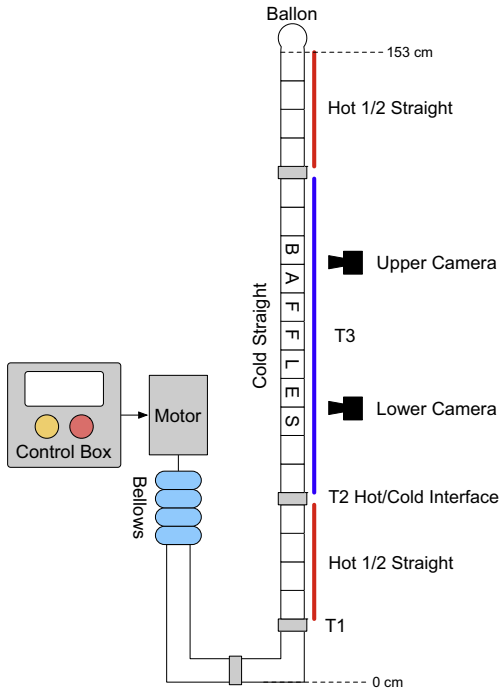

Fig. 1. Experimental setup showing positions of temperature measurement, cameras, glass sections and collars which connect the glass components together.

Table 1
Temperature profiles for high oscillation conditions (2 Hz, 45 mm) and low oscillation conditions (1 Hz, 45 mm).

Position on MFOBC	High oscillation	Low oscillation
*T*1 (°C), 16.5 cm	82	84.0
*T*2 (°C), 54.5 cm	26.8	29.5
Lower camera (°C), 66.5 cm	22.0	23.3
*T*3 (°C), 85.5 cm	19.5	19.8
Upper camera (°C), 88.0 cm	19.5	19.7
*T*4 (°C), 110 cm	23.7	24.6
*T*5 (°C), 134 cm	38.4	41.5

two half straights above and below are kept hot to prevent seeding from above and below, respectively. Temperatures *T*1 and *T*2 are monitored during experiments via built-in thermocouples. Temperatures *T*3, *T*4 and *T*5 are recorded for calibration purposes prior to the experiment as multiple thermocouples in the system may affect the fouling process.

Two sets of oscillation conditions were used for fouling experiments: high oscillation with frequency and amplitude of 2 Hz and 45 mm, respectively, and low oscillation with frequency and amplitude of 1 Hz and 45 mm, respectively. Table 1 gives temperature information pertaining to the two oscillation conditions used for the experiments.

L-Glutamic Acid (LGA) was crystallised from water in this setup. The supersaturations of the solutions were calculated from the solubility at 20 °C, which has a value of 7.07 g/L of water (Manzurola and Apelblat, 2002; Belitz et al., 2009). Supersaturations 3, 4 and 6 were used. Hot solution at 80 °C was prepared out with the MFOBC and pumped while hot in to the MFOBC using a peristaltic pump via a port at the base of the equipment. This was filled so that the upper half section was 75% full. At this point the oscillation was set and the experiment was run and images were taken. Two Microsoft LifeCam VX-3000 cameras were used and LED torch was used for illumination inside an enclosed environment to ensure constant lighting and to minimise reflections. The jacket temperatures of the glass straights were preset before being filled with hot solutions in order to quickly achieve the desired bulk solution temperatures. A balloon was placed over the top section of the MFOBC to eliminate effects from evaporation.

2.2. Image preprocessing

The web camera output is a series of JPEG images with resolution of 320×240 pixels. Each pixel consists of a tuple of the Red, Green and Blue 8-bit colour components. The 8-bit component values allow colour intensities to be captured in the range of 0 and 255, where 0 is no presence and 255 is the maximum presence of the corresponding component. A pixel with value $(R, G, B)=(255, 255, 255)$ represents a white pixel, while a pixel with value $(R, G, B)=(0, 0, 0)$ represents a black pixel.

The sequence of RGB JPEG images is converted to grey scale images using the formula $0.2989R+0.5870G+0.1140B$ which is the well accepted NTSC standard for luminance. The images are cropped to 100×100 pixels, with offset of 80 pixels from the top and 100 pixels from the left (shown in Fig. 2), in order to eliminate reflections from the cylindrical reactor walls. The exact location of cropping is not important as long as reflections due to the pipe curvature and the time stamp annotations are eliminated. As a result, the initial cropped frame has only black pixels (intensity 0) when the crystalliser has no growth in the bulk or walls. The cropping is performed in all images acquired and the resulting image sequence consists of a 3 dimensional array with $N=100$ rows by $M=100$ columns and K frames. The instantaneous intensity of a pixel at location (i, j) at time t is denoted by $I_{ij}(t)$.

2.3. Analysis methodology

Often experimentalists capture signal traces (profiles) and estimate induction time offline after the experiments are finished using a first order polynomial regression near the region of the crystal appearance. This kind of approach clearly does not allow early detection of crystal appearance and/or fouling events since an onset of change in relevant measurable quantities can only be determined after the extent of change becomes very significant. Moreover, choice of regression window can be arbitrary and often cannot be uniquely determined. An online real-time method to identify induction time is usually based on selection of a predetermined, fixed amplitude threshold and when the signal traces exceed that threshold, it is concluded that the induction time has been observed. Although this may be adequate for well characterised setups with known compounds and experimental conditions, it is impractical when applied to new systems or under different conditions or equipment. In order to address this challenge, a Bayesian Online Change Point Detection technique is presented in Section 2.4 for the automatic estimation of the induction time independent of setup, compound or conditions and it is agnostic of the signal trace used (i.e. sensor type). Its applicability for a wide range of signal traces is demonstrated throughout this work as it is the method chosen here to identify induction time in either bulk solution, at solid surfaces, or both combined.

Typical signal traces used to measure induction times are provided by Process Analytical Technology (PAT) equipment based on spectroscopic, scattering or video/imaging methods. However, such equipment is generally only able to detect induction time for crystal appearance in the bulk solution and in case signals from both bulk solution and vessel walls are recorded, it provides information on combined bulk and wall changes together. Some instruments such as the Mettler Toledo FBRM now provide a fouling index indicator for the probe window however these may not be representative of the encrustation levels experienced on the

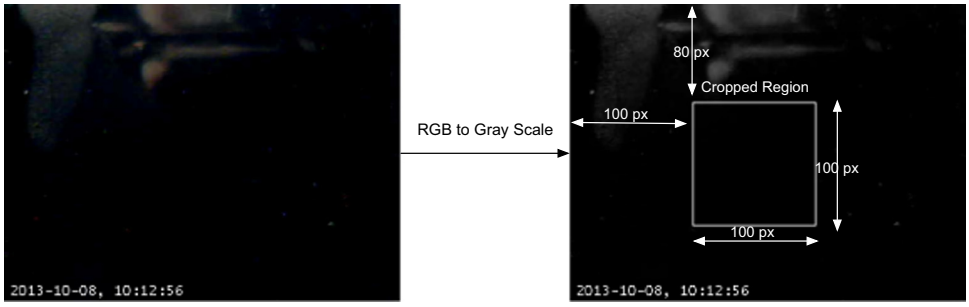

Fig. 2. Image pre-processing.

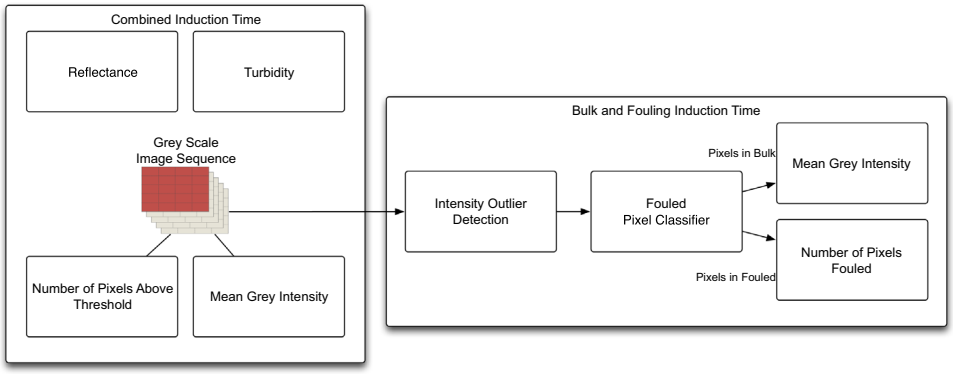

Fig. 3. Signals that can be used to estimate combined induction time and the proposed method to separate crystal appearance in the bulk solution and at the solid surfaces.

reactor walls, since probe coating materials are often different from those on the reactor walls hence varying the degree of encrustation. Some previous reports in the literature have employed imaging systems to estimate induction time (Simon et al., 2009a,b). These techniques are able to report in real-time the induction time using Mean Grey Intensity as a signal trace and amplitude thresholding as a detection method. Their performance is similar to that of PAT equipment such as ATR-IR (Simon et al., 2009a). Another rudimentary signal trace is to count the number of pixels above an intensity threshold. All the signal traces that can be used to measure combined induction time are illustrated in Fig. 3 and described in detail in Section 3.

Fig. 3 shows the proposed approach to detect separately crystal appearance in the bulk solution and on the vessel walls. The acquired images are initially passed through an Intensity Outlier Detector which highlights pixels with higher intensity. These pixels are subsequently processed by the Fouled Pixel Classifier that infers pixel state as fouled and non-fouled. The non-fouled pixels (i.e. in the bulk) are subsequently processed to generate the Mean Grey Intensity signal trace for estimation of the bulk induction time, while the fouled pixels are counted to provide a fouling index indicator and estimate the fouling induction time. The bulk and fouling induction time estimations are described in detail in Section 4.

2.4. Automatic change point detection

A typical progression profile from turbidity, reflectance or image Mean Grey Intensity start with low amplitude and as crystals appear, the amplitude rises. Induction times can be determined in a post-processing fashion after an experiment is completed or online, through thresholding the amplitude of the signal trace. Although these techniques are effective, they are sensitive to acquisition equipment and experimental conditions with parameter tuning necessary. In order to overcome these limitation, a Bayesian Online Change Point Detection (Adams and MacKay, 2007) approach is used here, modelling the data as a

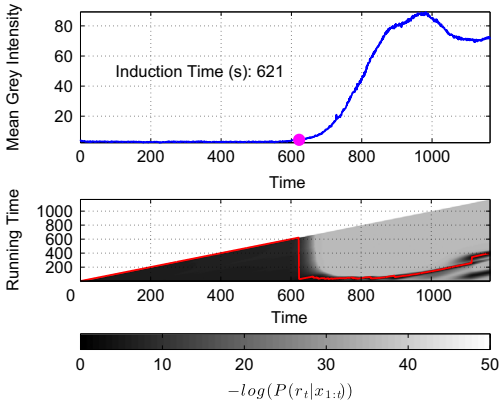

Fig. 4. Top: mean grey intensity profile against time. Bottom: The intensity plot shows the probability of the current run time $P(r_t|x_{1:t})$ at each time step (in logarithmic scale). The most probable run time r_t is annotated with the red line. (For interpretation of the references to color in this figure caption, the reader is referred to the web version of this article.)

Poisson process and the rate of exponential prior on the change point interval $\lambda_{gap} = 1000$ (i.e. change point distribution) in a similar fashion to the Coal Mine Disaster Data in Adams and MacKay (2007).

The top plot in Fig. 4 shows the MGI data of an experiment against time. For every new observation (i.e. MGI value), while the parameter η of the Poisson distribution remains the same, there is no occurrence of a change point and the run length increases by 1. When a new observation appears that comes from a Poisson with a different parameter η', the run time drops indicating a change point. The change point interval has rate λ_{gap} which models probabilistically the occurrence of a change point.

At the bottom graph of Fig. 4 the intensity plot shows the posterior probability of the current run length $P(r_t|x_{1:t})$ at each time step t using a logarithmic scale. Darker pixels indicate higher

probability while white pixels indicate zero probability. For a time step t, a column of pixels of the intensity plot illustrate the probability mass function for every run time/length.

For example, for $t=600$, the run time above 600 has zero probability and hence the $-\log(0)=\mathrm{Inf}$ which is shown as white. For run time below 600, the probability is between 0 and 1 which results in a shade of grey. The highest probability occurs at run time 600 which is the darkest pixel on that column and a change point has yet to occur. Similarly, for time $t=1000$, the maximum occurs at run length 140 (a number of change points have already occurred). The most probable run times are annotated with a red line on the bottom graph of Fig. 4.

The algorithm finds the negative slopes on the most probable run times (i.e. the points where the run time is reset) and these are the detected change points. The first change point is attributed to the onset of crystal formation. Subsequent change points are caused from breakage of encrusted regions and re-encrustation, but those are not considered in this analysis.

3. Combined induction time estimation

In this section, the Bayesian Online Change Point Detection algorithm is applied in a number of signal traces to estimate combined induction time. The algorithm is applied to turbidity, FBRM and image based signals as shown in Fig. 3.

As an example, consider a crystallisation experiment for LGA with concentration 45 g/L in water, oscillation amplitude of 30 mm and frequency 1.5 Hz. The measured profiles of the experimental signals are shown in Fig. 5. The induction times based on the algorithm presented in Section 2.4 using the FBRM and turbidity signal traces are 23.50 and 27.25 min respectively.

Previous applications of image processing to estimate induction time have proposed an automatic detection from Mean Grey Intensity (MGI) signal traces (Simon et al., 2009a,b). These works have identified that the size of the interrogation window affects the induction time estimation. Large windows spatially average a greater area and consequently, might miss the early appearance of crystals. On the counter side, small windows are prone to noise and other effects such as bubbles may lead to false detections.

Formally, the mean grey intensity $\bar{I}(t)$ for every frame at time $t\in\{1,2,\ldots,K\}$ is given as follows:

$$\bar{I}(t)=\frac{\sum_{i=1}^{N}\sum_{j=1}^{M}I_{ij}(t)}{NM} \tag{1}$$

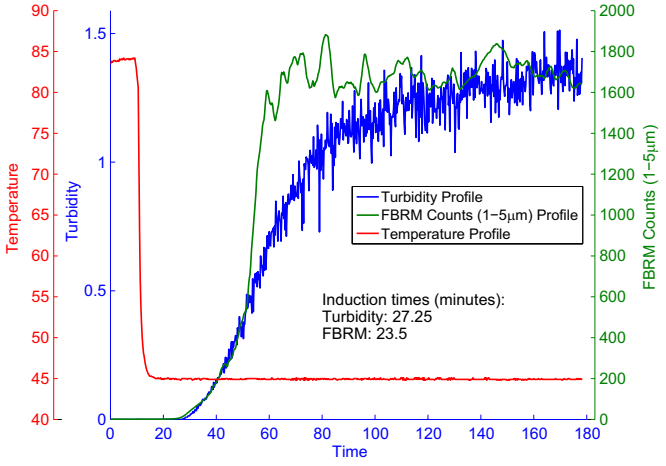

Fig. 5. Temperature, turbidity and FBRM signal traces for crystallisation of LGA in water (experiment with no fouling).

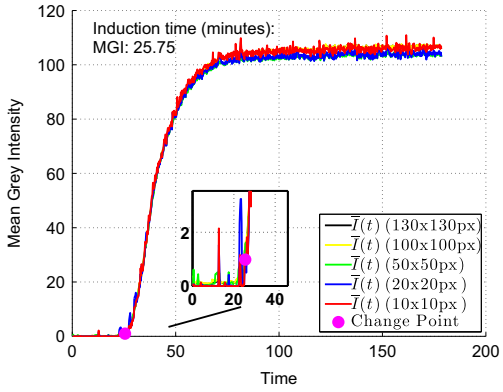

Fig. 6. Mean grey intensity profile for various interrogation window sizes. LGA in water (experiment with no fouling).

where $I_{ij}(t)$ is the instantaneous grey intensity of the pixel (i,j) at time t.

Often, the limitations of MGI traces are that it dampens the early detection of crystals that flow through the camera view finder making the method of estimating induction time through MGI is sensitive to the interrogation window size. The Mean Grey Intensity curves against time for various interrogation window sizes are shown in Fig. 6. The estimated induction time for all interrogation windows is 25.75 min and the effect of the window sizes is not significant. Unlike the work presented in Simon et al. (2009b) the camera resolution used here is low and individual crystals cannot be detected with confidence hence some sensitivity is lost. Also, the proposed change point detection algorithm estimates the induction time in a probabilistic fashion and even if there are some spikes in the waveform. For example for windows 10×10 pixels and 20×20 pixels, the waveforms have spikes before the detected induction point which was most likely caused from bubbles passing through the window.

Another method which could increase sensitivity compared to MGI is counting pixels above a threshold. Intuitively, the crystal appearance has started when the solution in the crystalliser gets cloudy i.e. the intensity of the pixels in the frame start to rise. Frequently experimentalists capture images at regular intervals to retrospectively verify the experiments. A standard method to determine process progression is to select an intensity threshold τ and at every time instance $t\in\{1,2,\ldots,K\}$, count the percentage of pixels exceeding the threshold[2]. More formally for a threshold $\tau\in\{1,2,\ldots,255\}$, the function counting the ratio of pixels above the threshold is

$$C_{\tau}(t)=\frac{\sum_{i=1}^{N}\sum_{j=1}^{M}u_{\tau}(I_{ij}(t))}{NM} \tag{2}$$

where $u_{\tau}(x)$ is the step function:

$$u_{\tau}(x)=\begin{cases}1 & \text{if } x\geq\tau\\ 0 & \text{if } x<\tau\end{cases} \tag{3}$$

Fig. 7(a) shows the percentage of pixels above the threshold τ versus time. Applying the change point detection method on the threshold signal traces indicates that the estimated induction varies significantly with the threshold value τ. The relation between τ and the estimated induction time is shown in Fig. 7 (b). The induction time increases almost linearly with the threshold. Low intensity thresholds provide high sensitivity however,

[2] *Note*: this threshold is applied on all pixels of every frame in the image sequence, unlike the MGI comparison threshold mentioned previously for detection purposes.

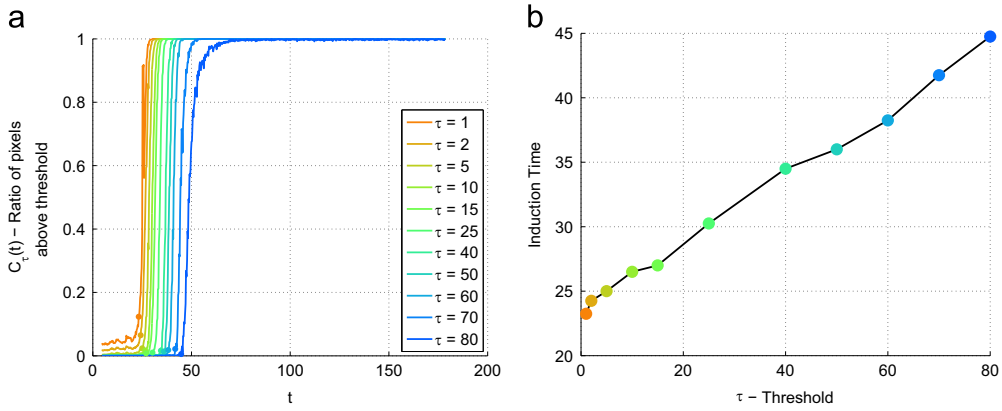

Fig. 7. LGA in water (experiment with no fouling): (a) Percentage of pixels above threshold τ versus time for various threshold levels. (b) Induction time for varying threshold levels.

Table 2
Comparison of induction time from various signal traces. LGA in water, (experiment with no fouling).

Parameter	Induction time (min)
FBRM	23.50
MGI	25.75
Turbidity	27.25
Pixel thresholding	(23.25–44.75) Varying with threshold τ

application of this technique on other datasets with higher image noise, and did not provide a robust estimation. Low thresholds produce to spiky signal traces, especially during the beginning of the experiment where camera noise is significant leading to incorrect estimation of induction time. For high thresholds, the crystal appearance must be well developed in order to observe a waveform rise.

The combined induction times obtained from various signal traces when the Bayesian Online Change Point Detection algorithm is applied are summarised in Table 2. FBRM signal traces are the most sensitive followed by the MGI and Turbidity.

The turbidity probe has no means to detect fouling and hence measure the combined induction time. The FBRM probe is able to distinguish encrustation on the probe through fouling index however, does not capture any information related to fouling on the crystalliser walls.

Estimating induction time through imaging contains information related to the fouling of the crystalliser walls, however this information is not being utilised.

4. Fouling and bulk induction time

Images from a commodity web camera pointing towards the crystalliser walls do not only contain information about crystal appearance in the bulk but also the crystalliser walls. This section presents a method to separate fouling and bulk induction time through statistical analysis of the acquired images as summarised in Fig. 3.

Crystals moving through the camera view result in variations in pixel intensity. Regions where crystals are present will have higher pixel intensity compared to background regions. Crystals stuck on the crystalliser walls are closer to the camera viewfinder and reflect more light. Crystals in the bulk also reflect light leading to high pixel intensities, however the pixel intensities are not consistently high for a consecutive number of frames. As the crystals move away with the liquid flow intensities drop. The proposed pixel detection algorithm consists of two steps:

1. Identify pixels with the highest intensity.
2. Identify pixels which have the highest intensity for a consecutive number of frames. This rule in necessary to avoid false positives where particles larger/brighter than the encrusted region are passing through the view.

To achieve the first step of the process an upper outlier detection method based on Chebyshev's inequality is used (Amidan et al., 2005). The inequality provides a bound on the percentage of data point falling further than k standard deviations away from the mean. On this occasion the inequality is applied to the pixel intensities distribution of the frame at time t:

$$P(|I(t)-\bar{I}(t)| \geq k\sigma) \leq \frac{1}{k^2} \tag{4}$$

The inequality is used to determine upper and lower Outlier Detection Value (ODV) limits (ODV_U and ODV_L) and does not make any assumptions on the underlying data distribution. Pixels with intensity outside the limits are classified as outliers. For $k=5$ this leads to maximum 4% of pixels been classified as outliers on both directions. The outlier detection limits are given by

$$ODV_L = \bar{I}(t) - k\sigma$$
$$ODV_U = \bar{I}(t) + k\sigma \tag{5}$$

From these two detection values, only upper outliers (greater than ODV_U) indicate fouled regions and the following detection function is defined:

$$d_{ij}(t) = \begin{cases} I_{ij} & \text{if } I_{ij} \geq ODV_U \\ -Inf & \text{otherwise} \end{cases} \tag{6}$$

The detection function has a value of $-\text{Inf}$ for pixels that are not detected as outliers while the detection function is equal to the corresponding pixel intensity (I_{ij}).

Fig. 8 shows the MGI profile curve in red line, while the grey shaded area shows the intensities that lie between the Outlier Detection Value Lower (ODV_L) and the Outlier Detection Value Upper (ODV_U) from Eq. (5). The green line shows the instantaneous pixel intensity of an arbitrary pixel at location (104, 117). Every time pixel intensity exceeds the ODV_U, the pixel is classified as an outlier as in Eq. (6) and is annotated on the graph with black crosses. All pixels that have intensity lower than the upper bound ODV_U have detection value of $-Inf$. Not all pixels that the detection function has identified as outliers are necessarily fouled. The high intensity can be caused either due to camera noise or objects passing through that pixel region. However, pixels that the detection function has consistently identified as outliers; i.e. for N_S

consecutive number of frames, are fouled and the following filtering algorithm is used to detect those:

1. For time step t, create a set $\mathcal{A}(t)$ with all pixels in the frame

$$\mathcal{A}(t) : \{(i,j)\}, \quad \text{for all } i \in \{1,\ldots,N\} \text{ and } j \in \{1,\ldots,M\} \tag{7}$$

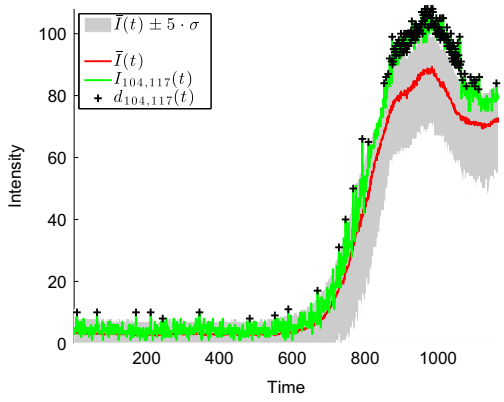

Fig. 8. Mean grey intensity profile with Chebyshev's outlier detection bounds for $k=5$. The green line shows the instantaneous intensity of pixel (104, 117), while the black crosses indicate the points where the pixel intensity has exceeded the ODV_U; i.e. the output of the $d_{ij}(t)$ from Eq. (6). LGA in water (experiment with fouling). (For interpretation of the references to color in this figure caption, the reader is referred to the web version of this article.)

2. Using the set $\mathcal{A}(t)$ estimate the ODV_U required for the outlier detection function in Eq. (6).
3. Create a set $\mathcal{F}(t)$ with all the pixels that their d_{ij} is greater than or equal to 0 for the previous $N_S=5$ time steps/frames. Essentially, this steps looks to previous images to determine if the pixels where consistently an outlier based on the instantaneous detection function.

$$\mathcal{F}(t) : \{(i,j)\} \quad \text{where } d_{ij}(t-l) \geq 0, \quad \text{for all } l \in \{1,\ldots,N_S\},\ i \in \{1,\ldots,N\},\ j \in \{1,\ldots,M\} \tag{8}$$

4. The number of fouled pixels is equal to cardinality (number of elements) of the set $\mathcal{F}(t) : |\mathcal{F}(t)|$.
5. Recompute ODV_U for the set of pixels in the intersection $\mathcal{A}(t) \cap \overline{\mathcal{F}(t)}$ (i.e. exclude pixels that were classed as fouled in the current time t).
6. Go to step 3.

The output of the classification algorithm can subsequently be used to visualise regions where fouling has occurred. Fig. 9 shows two example images and their corresponding outputs of the classifier.

Fig. 10 shows the percentage of pixels classified as fouled, against time which is obtained as the ratio of the cardinality of the set $\mathcal{F}(t)$ over the total number of pixels in the frame. The percentage of pixel can be used as a fouling index indicator at any stage of the experiment. Fig. 10 also shows the combined MGI signal trace i.e. without taking in consideration the pixel class as in Section 3, while the MGI bulk signal

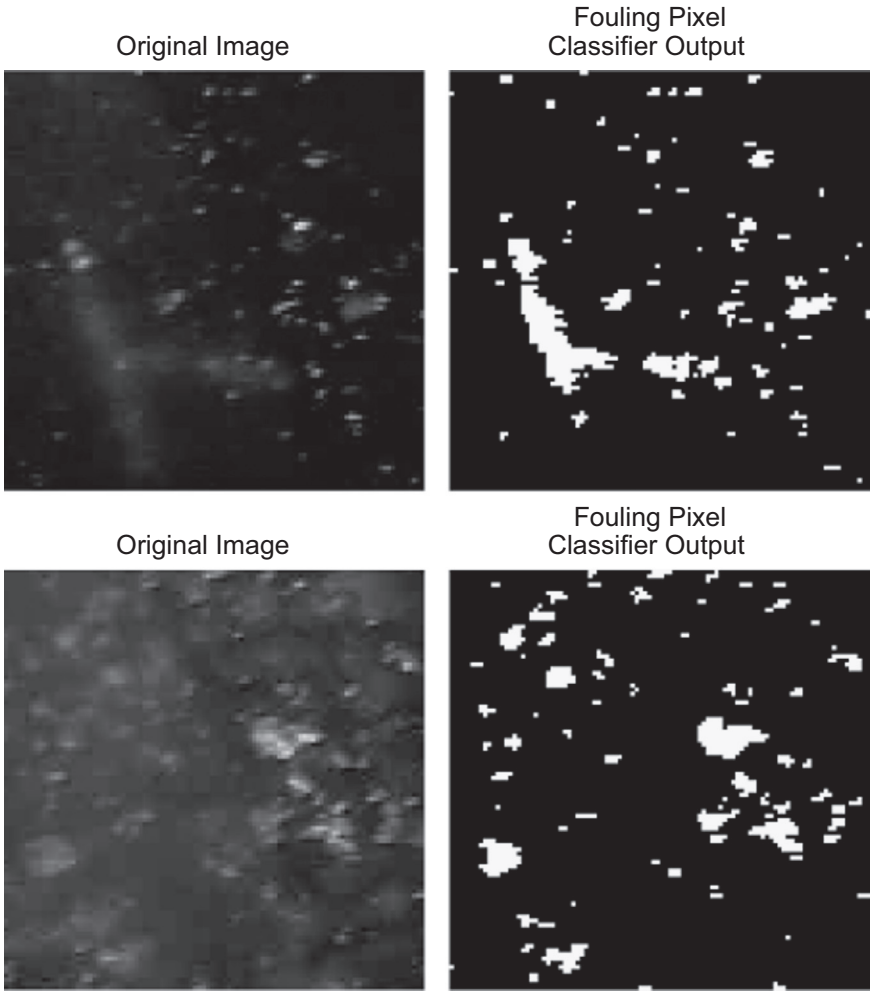

Fig. 9. Two examples of original images and outputs of the fouling classifier. LGA in water (experiment with fouling).

trace only considers pixels that are not fouled (i.e. belonging to the bulk).

In this experiment, the combined MGI and Bulk MGI are almost identical and this is due to a low number of fouled pixels (i.e. only 2% of pixels are fouled). Using the change point detection to estimate induction times from these signal traces, fouling appears at 575 s, while induction in the bulk occurs at 621 s, with identical time for the combined trace.

It is important to highlight that the fouling induction time is detected before bulk or combined induction times. This is justified when considering that the fouling signal trace provides higher sensitivity when compared to MGI traces. The MGI traces inherently damp localised changes until the intensity of a significant number of pixels has increased. This difference in sensitivity introduces a potential uncertainty of the order of events, e.g., when induction times on the wall and in the bulk are near each other. The aim in this work is to provide an early warning system for fouling and this is achieved through the high sensitivity provided by the fouling signal trace. Measuring bulk induction time with high sensitivity could be achieved through the use of other PAT equipment such as reflectance (i.e. FBRM).

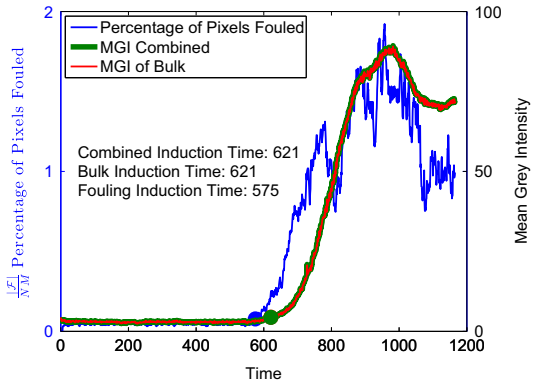

Fig. 10. Signal trace profiles for fouling index, bulk MGI and combined MGI. LGA in water (experiment with fouling).

4.1. Sensitivity of fouling classifier parameters

The fouling pixel classifier sensitivity can be adjusted through two parameters: the outlier detection sensitivity (k standard deviations) and the number of consecutive frames (N_S) a pixel has to remain an outlier before it is classified as fouled.

Fig. 11(a) shows the percentage of pixels against time for various k standard deviations and $N_S=5$. The maximum percentage of pixels intensities beyond $k=2$ standard deviations from the mean is 25% hence a greater number of pixels have the potential to be identified from the detection function in Eq. (6). Higher values of k restrict the bound and hence the sensitivity of the detection function. For $k=6$ the maximum percentage of pixels is restricted to 2.77%. The fouling induction time against k is shown in Fig. 11(b). For $k=2$ the bound is wide and pixels in the bulk are classified prematurely as fouled. However, as the k increases to 3 and beyond the sensitivity reduces resulting in identical induction times.

Similar sensitivity analysis is performed for N_S; the number of consecutive frames a pixel has to be identified an outlier for a fixed

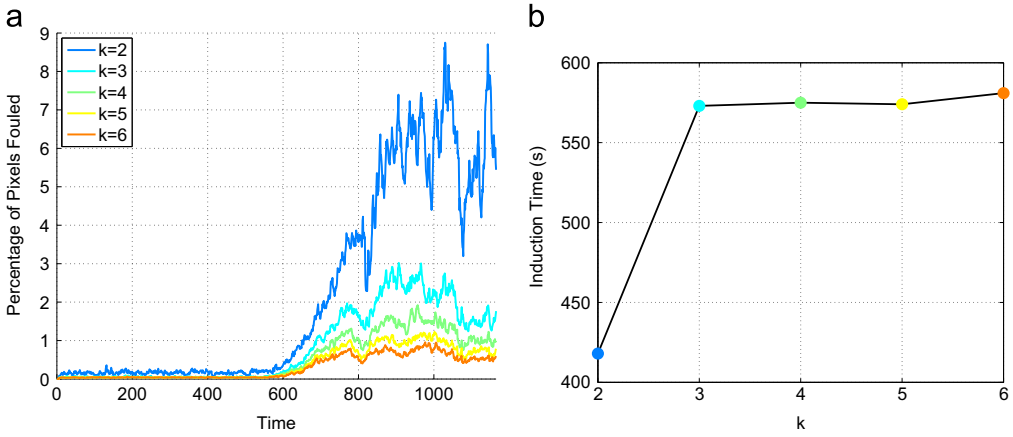

Fig. 11. (a) Percentage of fouled pixels versus time for various k. (b) Induction time against k.

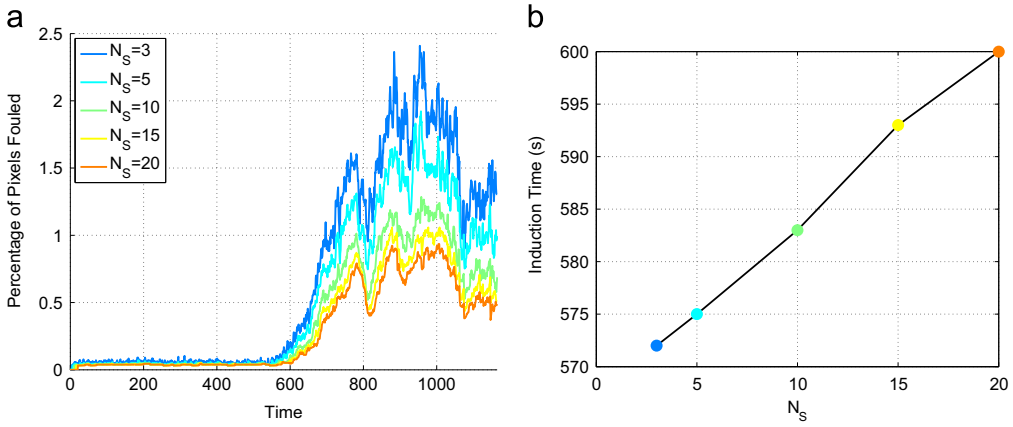

Fig. 12. (a) Percentage of fouled pixels versus time for various N_S. (b) Induction time against N_S.

value of $k=5$. The percentage of fouled pixels against time is shown in Fig. 12(a). The longer the time period a pixel remains an outlier the more severe the fouling. As expected, the lower the N_S the greater the chances that the pixel intensity is an outlier and consequently highlighted as fouling. As the N_S increases pixels have to remain outliers for a longer period of time. The fouling induction time against N_S is shown in Fig. 12(b). It should be noted that although the algorithm is sensitive to the selection of the N_S parameter, the relative change in induction time is less the 5% of the absolute induction time. Inspection of the acquired images indicates that parameters $k=5$ and $N_S=5$ are the most suitable to detect fouled pixels regions.

5. Conclusions

In this paper we presented a method to automatically detect induction time through Bayesian Online Change Point Detection in real-time while the experiment is in progress. It is demonstrated that the change point detection algorithm can estimate induction time for various types of signal traces such as reflectance, turbidity, Mean Grey Intensity and percentage of pixels fouled without the need to tune model parameters. This approach to estimating induction time is more robust than thresholding where the estimates can vary significantly with the threshold selection.

We have also developed a novel method for the early detection of fouling through commodity web cameras. Classification of image pixels corresponding to either bulk solution or fouled surface was achieved through statistical analysis of pixel intensity time series. The proposed technique is applicable to industrial settings where the visual access to the fouling surface is available.

The number of pixels classified as fouled is an indicator of the degree of fouling at every stage of the experiment. Using the fouling indicator and applying the automatic change point detection, fouling induction time can be estimated. We note that surface fouling and bulk crystallisation signal traces provide significantly different sensitivity and that may introduce an uncertainty in the order of events when induction times at surface and in the bulk are close to each other.

Acknowledgements

The authors would like to acknowledge financial support from the EPSRC, AstraZeneca and GSK. This work was performed as part of the “Intelligent Decision Support and Control Technologies for Continuous Manufacturing and Crystallisation of Pharmaceuticals and Fine Chemicals” (ICT-CMAC) Project (grant number EP/K014250/1).

Appendix A. Supplementary data

Supplementary data associated with this paper can be found in the online version at http://dx.doi.org/10.1016/j.ces.2015.01.038.

References

Adams, R.P., MacKay, D.J.C., 2007. Bayesian Online Changepoint Detection. Cambridge, UK.
Amidan, B.G., Ferryman, T.A., Cooley, S.K., 2005. Data outlier detection using the Chebyshev theorem. In: 2005 IEEE Aerospace Conference, 3814-3819, http://dx.doi.org/10.1109/AERO.2005.1559688.
Belitz, H.-D., Grosch, W., Schieberle, P., 2009. Food Chemistry, 4th edition Springer, Heidelberg.
Bott, T.R., 1997. Aspects of crystallisation fouling. Exp. Thermal and Fluid. Sci. 14, 356–360.
Brown, C.J., Ni, X.-W., 2011. Online evaluation of paracetamol antisolvent crystallization growth rate with video imaging in an oscillatory baffled crystallizer. Cryst. Growth Des. 11, 719–725.
Förster, M., Augustin, W., Bohnet, M., 1999. Influence of the adhesion force crystal/heat exchanger surface on fouling mitigation. Chem. Eng. Process.: Process Intensif. 38, 449–461.
Geddert, T., Bialuch, I., Augustin, W., Scholl, S., 2009. Extending the induction period of crystallization fouling through surface coating. Heat Transf. Eng. 30, 868–875.
Geddert, T., Augustin, W., Scholl, S., 2011a. Induction time in crystallization fouling on heat transfer surfaces. Chem. Eng. Technol. 34, 1303–1310.
Geddert, T., Augustin, W., Scholl, S., 2011b. Influence of surface defects and aging of coated surfaces on fouling behavior. Heat Transf. Eng. 32, 300–306.
Manzurola, E., Apelblat, A., 2002. Solubilities of L-glutamic acid, 3-nitrobenzoic acid, p-toluic acid, calcium-l-lactate, calcium gluconate, magnesium-dl-aspartate, and magnesium-l-lactate in water. J. Chem. Thermodyn. 34, 1127–1136.
Moscosa-Santillán, M., Bals, O., Fauduet, H., Porte, C., Delacroix, A., 2000. Study of batch crystallization and determination of an alternative temperature-time profile by on-line turbidity analysis—application to glycine crystallization. Chem. Eng. Sci. 55, 3759–3770.
Mullin, J.W., 2001. Crystallization, 4th edition Butterworth Heinemann, London, UK.
Nagy, Z.K., Fevotte, G., Kramer, H., Simon, L.L., 2013. Recent advances in the monitoring, modelling and control of crystallization systems. Chem. Eng. Res. Des. 91, 1903–1922.
Ni, X.-W., 2006. Continuous oscillatory baffled reactor technology. Innov. Pharm. Technol., 8–12.
Oliveira, M.S.N., Fitch, A.W., Ni, X.-W., 2003. A study of bubble velocity and bubble residence time in a gassed oscillatory baffled column—effect of oscillation frequency. Chem. Eng. Res. Des. 81, 233–242.
Raphael, M., Rohani, S., 1996. On-line estimation of solids concentrations and mean particle size using a turbidimetry method. Powder Technol. 89, 157–163.
Simon, L.L., Nagy, Z.K., Hungerbuhler, K., 2009a. Endoscopy-based in situ bulk video imaging of batch crystallization processes. Org. Process Res. Dev. 13, 1254–1261.
Simon, L.L., Nagy, Z.K., Hungerbuhler, K., 2009b. Comparison of external bulk video imaging with focused beam reflectance measurement and ultra-violet visible spectroscopy for metastable zone identification in food and pharmaceutical crystallization processes. Chem. Eng. Sci. 64, 3344–3351.
Simon, L.L., Abbou Oucherif, K., Nagy, Z.K., Hungerbuhler, K., 2010a. Bulk video imaging based multivariate image analysis, process control chart and acoustic signal assisted nucleation detection. Chem. Eng. Sci. 65, 4983–4995.
Simon, L.L., Oucherif, K.A., Nagy, Z.K., Hungerbuhler, K., 2010b. Histogram matching, hypothesis testing, and statistical control-chart-assisted nucleation detection using bulk video imaging for optimal switching between nucleation and seed conditioning steps. Ind. Eng. Chem. Res. 49, 9932–9944.
Simon, L.L., Merz, T., Dubuis, S., Lieb, A., Hungerbuhler, K., 2012. In situ monitoring of pharmaceutical and specialty chemicals crystallization processes using endoscopy–stroboscopy and multivariate image analysis. Chem. Eng. Res. Des. 90, 1847–1855.
Stonestreet, P., Harvey, A.P., 2002. A mixing-based design methodology for continuous oscillatory flow reactors. Chem. Eng. Res. Des. 80, 31–44.
Vendel, M., Rasmuson, A.C., 1997. Mechanisms of initiation of incrustation. AIChE J. 43, 1300–1308.
Wallhäußer, E., Hussein, M., Becker, T., 2012. Detection methods of fouling in heat exchangers in the food industry. Food Control 27, 1–10.